Available online at www.sciencedirect.com

ScienceDirect

Scripta Materialia 81 (2014) 48–51

Scripta MATERIALIA

www.elsevier.com/locate/scriptamat

High-coercivity hot-deformed Nd–Fe–B permanent magnets processed by Nd–Cu eutectic diffusion under expansion constraint

T. Akiya,[a] J. Liu,[a,b] H. Sepehri-Amin,[a] T. Ohkubo,[a] K. Hioki,[c] A. Hattori[c] and K. Hono[a,b,*]

[a]*Elements Strategy Initiative Center for Magnetic Materials, National Institute for Materials Science, Tsukuba 305-0047, Japan*

[b]*Graduate School of Pure and Applied Science, University of Tsukuba, Tsukuba 305-8577, Japan*

[c]*Daido Steel Co. Ltd., Nagoya 457-8545, Japan*

Received 12 February 2014; revised 2 March 2014; accepted 2 March 2014
Available online 7 March 2014

The application of expansion constraint during the grain-boundary diffusion process using $Nd_{70}Cu_{30}$ eutectic alloy minimizes the remanence loss for the coercivity enhancement by optimizing the volume fraction of the Nd(Cu)-rich non-ferromagnetic intergranular layer. The diffusion-processed sample exhibits $\mu_0 H_c \sim 2$ T, $\mu_0 M_r = 1.36$ T and $(BH)_{max} = 358$ kJ m^{-3} at room temperature. Because of the low-temperature coefficient of coercivity, the magnet showed $(BH)_{max} \sim 191$ kJ m^{-3} at 200 °C, which is superior to that of Dy-containing high-coercivity sintered magnets.

Keywords: Permanent magnet; Coercivity; Nd-Fe-B; Hot-deformed magnet; Diffusion process

Due to the recently emerging concern regarding the stable supply of heavy rare-earth elements (HRE), such as Dy and Tb, considerable effort has been devoted to increasing the coercivity of Nd–Fe–B magnets without using HRE. In such applications as the traction motors of electric vehicles and wind-turbine generators, the temperature of the magnets rises to nearly 200 °C due to the evolution of eddy currents. Thus, $(Nd_{0.7}Dy_{0.3})$–Fe–B-based magnets with sufficiently high intrinsic coercivities ($\mu_0 H_c > 0.8$ T) and energy densities ($(BH)_{max} > 150$ kJ m^{-3}) at 200 °C are currently used for these applications. The purpose of this study is to explore the possibility of developing high-coercivity and high-energy-density Nd–Fe–B magnets without using HRE.

The coercivity of Nd–Fe–B sintered magnets is empirically known to increase with decreasing grain size of the main $Nd_2Fe_{14}B$ phase [1–4]. Recently, Sagawa et al. reported a high coercivity of 2 T by refining the grain size of the sintered magnets to 1 μm by a pressureless sintering process, by which the oxygen atmosphere was rigorously controlled in a completely closed processing system [5]. However, the reduction of the grain size further below 1 μm is technologically challenging because of the explosive nature of fine powders of rare earth alloys. On the other hand, the hot deformation of consolidated melt-spun Nd–Fe–B alloy flakes leads to the formation of ultrafine, platelet-shaped grains of ~300 nm in width and 50 nm in height without oxygen exposure of the individual grains [6]. The hard magnetic properties of such hot-deformed anisotropic magnets are comparable to those of Nd–Fe–B sintered magnets, i.e. $\mu_0 H_c \sim 1.2$ T and $\mu_0 M_r \sim 1.4$ T [7,8]. However, considering the ultrafine grain size compared to the single domain size of the $Nd_2Fe_{14}B$ phase, the coercivity of 1.2 T is too low. In spite of many attempts at increasing the coercivity of hot-deformed magnets, the reported maximum coercivity for a relatively Nd-rich composition barely exceeds 1.8 T without the addition of Dy [8–10].

One possible reason for the disappointedly low coercivity for their fine grain size is the exchange coupling of the $Nd_2Fe_{14}B$ grains of the hot-deformed magnet through a ferromagnetic intergranular phase [11]. Sepehri-Amin et al. [12] and Mishima et al. [13] independently reported substantial enhancements in

* Corresponding author at: National Institute for Materials Science, Tsukuba 305-0047, Japan; e-mail: kazuhiro.hono@nims.go.jp

http://dx.doi.org/10.1016/j.scriptamat.2014.03.002
1359-6462/

the coercivity of hydrogen-desorption-disproportionate-recombined processed magnet powders by forming an Nd-rich intergranular phase using Nd–Cu eutectic alloys as a diffusion source. We have recently extended this eutectic diffusion process to anisotropic hot-deformed magnets, demonstrating a dramatic increase in the coercivity to 2.3 T using $Nd_{70}Cu_{30}$ [14] and 2.6 T using $Nd_{60}Dy_{20}Cu_{20}$ as the diffusion sources [15]. We also observed a notable sample expansion only in the *c*-axis direction when the eutectic diffusion process was applied to a bulk hot-deformed sample [16], i.e. an 11.2% expansion was observed in the *c*-axis direction when $Nd_{70}Cu_{30}$ alloy was diffused at 650 °C for 3 h. Because of the volume expansion due to the infiltration of non-ferromagnetic $Nd_{70}Cu_{30}$, the magnetization decreases after the eutectic diffusion process. For use as high-performance magnets for motor applications, both the coercivity and the remanence or the energy density must be optimized at an elevated temperature of ~200 °C. In this study, we have applied a constraint to the volume expansion along the *c*-axis during the eutectic diffusion process to achieve a high coercivity without HRE while keeping the remanence loss at a minimum.

Hot-deformed magnets with a nominal composition of $Nd_{12.9}Fe_{77.2}Co_{3.9}B_{5.5}Ga_{0.5}$ in at.% or $Nd_{28.6}Fe_{66.5}Co_{3.5}B_{0.9}Ga_{0.5}$ in mass%, with initial dimensions of 7.01 × 7.01 × 5.60 (easy axis) mm^3, were used. As a diffusion source, melt-spun $Nd_{70}Cu_{30}$ ribbons were ball-milled in butoxyethanol. The bulk hot-deformed magnet samples were dipped into the butoxyethanol suspension with $Nd_{70}Cu_{30}$ particles of ~5 μm. Nd–Cu powder was additionally applied to the surface of the magnets to optimize the amount of the diffusion source. To constrain to the anisotropic expansion in the *c*-axis direction, the coated samples were placed between two stainless plates, as illustrated in the inset in Figure 1. The width of the clearance gap between the stainless-steel plates was adjusted using spacers. In this experiment, the initial sample thickness was 5.6 mm, and we used a clearance gap of 6.0 mm, allowing for 6.7% expansion. The diffusion process was performed at 650 °C for 3 h under a vacuum of 10^{-4} Pa. The bulk samples were observed by scanning electron microscopy backscattered electron (BSE) imaging using a Carl Zeiss CrossBeam 1540EsB at an accelerating voltage of 2.0 kV. X-ray diffraction analyses were performed using a Rigaku SmartLab with Cu K_α radiation. The magnetic properties were measured using a closed-circuit-type BH tracer after magnetization by a pulsed field of 7 T. High-temperature magnetic properties from 27 to 327 °C were estimated using a SQUID-VSM instrument. The demagnetization field correction of the obtained hysteresis curves were performed based on the magnetization curve measured using a closed-circuit-type BH tracer.

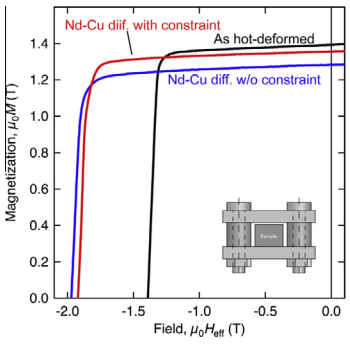

Figure 1. Demagnetization curves of the original hot-deformed sample and the samples that were diffusion-processed with and without an expansion constraint. The inset schematically shows how the expansion was constrained. (Color online).

The demagnetization curves of the original hot-deformed magnet and of the samples treated with the eutectic diffusion process with and without the expansion constraint are shown in Figure 1, and their magnetic properties are summarized in Table 1. In the original hot-deformed sample, the coercivity and the remanence were $\mu_0 H_c = 1.40$ T and $\mu_0 M_r = 1.39$ T, respectively. After the eutectic diffusion process without the expansion constraint, the coercivity was enhanced to $\mu_0 H_c = 1.97$ T at the expense of the remanence, $\mu_0 M_r = 1.27$ T. When the diffusion process is applied under the expansion constraint, nearly the same coercivity of $\mu_0 H_c = 1.92$ T was obtained with a relatively small decrease in the remanence to $\mu_0 M_r = 1.36$ T. These results imply that a higher remanence with a comparable coercivity is achieved by the eutectic diffusion process with an expansion constraint. As a result, the maximum energy product is also maintained at the value of $(BH)_{max} = 358$ kJ m^{-3}.

The expansion of the hot-deformed magnet was observed after the eutectic diffusion process. Without the expansion constraint, the sample expanded by 8%, from 5.60 to 6.09 mm, but only in the *c*-axis direction. On the other hand, expansions were observed not only in the *c*-axis direction but also in the perpendicular direction to the *c*-axis when an expansion constraint was applied. The sample expanded to the gap clearance of 6.02 mm in the *c*-axis direction, and it expanded from 7.01 to 7.09 mm in the ⟨0 0 1⟩ direction. This lateral expansion was not observed in the sample diffusion-processed without a constraint.

Typical BSE images of the three samples are shown in Figure 2. The dark and bright regions are the $Nd_2Fe_{14}B$ phase and the Nd-rich grain-boundary phase, respectively. In the original hot-deformed sample ((a) and (b)), the areal fraction of the Nd-rich intergranular phase was measured to be ~3%. From the weak contrast of the intergranular phase, the $Nd_2Fe_{14}B$ grains are considered to be exchange coupled [8]. In addition to the well-aligned platelet-like grains shown in Figure 2(a), zones containing equiaxed grains without [0 0 1] texture were also observed near the original ribbon interfaces (not shown) [15]. The volume fraction of the Nd-rich intergranular phase notably increases after the diffusion process, as shown in Figure 2(c) and (d). The areal fraction of the Nd(Cu)-rich phase estimated from the BSE image was ~18%. The thickness of the Nd-rich phase is increased along the *c*-axis direction, distinctly separating the $Nd_2Fe_{14}B$ grains in the direction normal to the flat surfaces of the platelets. However, the intergranular phase is not observed clearly along the long axis of the platelets. Some of the flat surfaces in Figure 2(c) are misaligned from other flat surfaces, i.e. the *c*-axis, which are misaligned in the diffusion-processed sample. This is another reason for the reduction in the remanence in addition to the increased volume fraction of the non-ferromagnetic

Table 1. Dimensions and magnetic properties of the samples studied.

Sample	Dimensions (mm)	Weight change	$\mu_0 M_r$ (T)	$\mu_0 H_c$ (T)	$(BH)_{max}$ (kJ m^{-3})
Initial	5.60 × 7.01 × 7.01	–	1.392	1.40	375
Conventional	6.09 × 7.01 × 7.02	+10.5%	1.270	1.97	306
Constrained	6.03 × 7.09 × 7.09	+8.0%	1.356	1.92	358

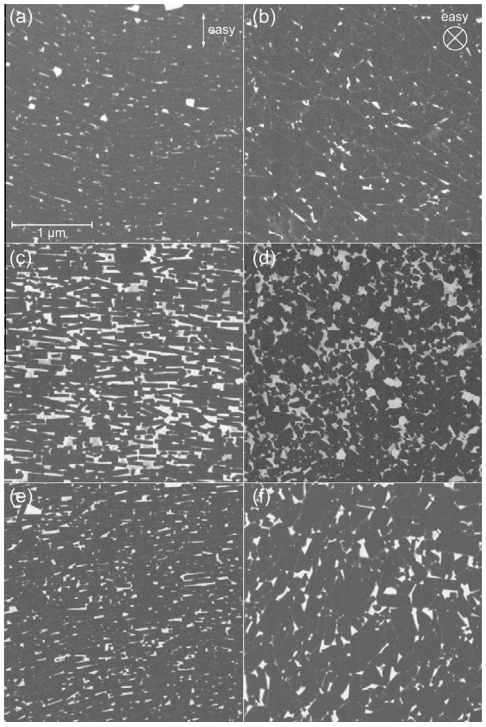

Figure 2. Backscattered electron images of the original hot-deformed (a, b), diffusion-processed (c, d) and diffusion-processed with an expansion constraint (e, f) samples. The left and the right rows are side views and plan views, respectively.

Nd(Cu)-rich intergranular phase. Figure 2(e) and (f) shows side and plan views of the hot-deformed magnet that was diffusion-processed under the expansion constraint. Compared to the sample diffusion-processed without a constraint, the volume fraction of the Nd(Cu)-rich phase is apparently smaller; the areal fraction of the Nd(Cu)-rich phase was ~8%. The coercivity is comparable to that of the diffusion-processed sample without a constraint, suggesting that the volume fraction of the Nd(Cu)-rich intergranular phase in the diffusion-processed sample without an expansion constraint is more than that required for enhancing the coercivity, which gives rise to the reduction of the remanence.

The weight increase and the reduction of the remanence by the diffusion process without an expansion constraint were +10.5 and −8.8%, respectively. On the other hand, the weight gain and the reduction of the remanence of the sample diffusion-processed with an expansion constraint were +8.0 and −2.6%, respectively. Compared to the weight gain by the Nd–Cu diffusion, the reduction of the remanence is much smaller. The remanence, M_r, of permanent magnets is given by:

$$M_r = f \times v \times M_s, \quad (1)$$

where f is the angular distribution of the c-axis of the hard phase, with $f = 0.5$ for randomly oriented grains and $f = 1$ for perfectly (001) textured polycrystalline magnets, v is the volume fraction of the $Nd_2Fe_{14}B$ phase and M_s is the saturation magnetization of $Nd_2Fe_{14}B$ [17]. Figure 3(a) compares the θ–2θ X-ray diffraction patterns of the original hot-deformed and diffusion-processed samples with and without an expansion constraint. In the original hot-deformed sample, all of the observed peaks are indexed as $Nd_2Fe_{14}B$, and the intensity ratio suggests a strong (001) texture of the $Nd_2Fe_{14}B$ grains. In the diffusion-processed magnet, we observed well-aligned $Nd_2Fe_{14}B$ peaks and extra peaks at approximately $2\theta = 25$ and 52°. These extra peaks are identified as the (011) and (022) peaks of the NdCu phase (*oP8*). However, in the sample diffusion-processed with an expansion constraint, the intensity of the peaks from the NdCu phase was reduced to nearly half of the original intensity, suggesting that the volume fraction of the Nd–Cu phase was reduced by the expansion constraint. The rocking curves from the (006) reflection for the three samples are shown in Figure 3(b). The full width at half maximum value for the original hot-deformed sample was $\Delta\theta = 8.60°$. After the eutectic diffusion process without an expansion constraint, the Δθ increased to 9.26°, indicating that the slight misalignment of the $Nd_2Fe_{14}B$ grains occurred during the diffusion process due to the presence of the Nd–Cu liquid. On the other hand, $\Delta\theta = 7.64°$ for the sample diffusion-processed with the expansion constraint. The reduction of Δθ from the original hot-deformed state implies that the alignment of $Nd_2Fe_{14}B$ grains was improved by the eutectic diffusion process with the expansion constraint. The high observed remanence in the sample diffusion processed with the expansion constraint is partly attributed to the improved c-axis texture of the platelet-like $Nd_2Fe_{14}B$ grains.

For the application of traction motors in electric vehicles, we must evaluate the coercivity as well as the energy density of the magnets at an elevated temperature of ~200 °C. Figure 4(a) shows the temperature dependence of the coercivity of the original hot-deformed sample and the samples that were diffusion-processed with and without constraints. To benchmark

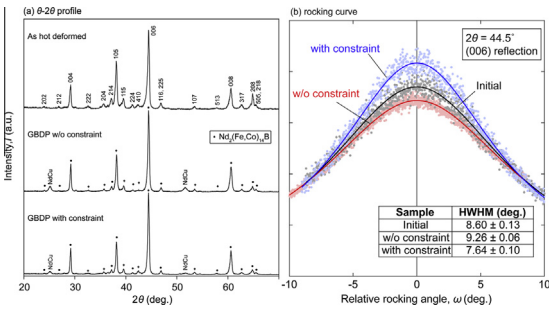

Figure 3. (a) θ–2θ profiles of the easy plane for the original hot-deformed, conventionally Nd–Cu diffused and Nd–Cu diffused with a constraint samples by X-ray diffraction. (b) Rocking curves for the (006) reflection of the three samples. (Color online).

these samples against the currently used (Nd, Dy)–Fe–B sintered magnets, the coercivities for 0% Dy, 4% Dy and 8% Dy class commercial sintered magnets are also shown [18]. The room-temperature coercivity of the diffusion-processed hot-deformed magnet is nearly the same as that of the 4% Dy sintered magnet. However, the temperature coefficient of the coercivity of the hot-deformed magnet,

$$\beta = \frac{\Delta H_c}{\Delta T} \times \frac{100}{H_c(20\,^\circ C)} \qquad (\Delta T = 20\text{–}140\,^\circ C), \qquad (2)$$

is −0.45, the absolute value of which is significantly lower than that for the sintered magnets (β ∼ −0.6) because of the small grain size. The typical grain size for the commercial sintered magnets is ∼5 μm, whereas that of the hot-deformed magnets is only 0.3 μm. Because the stray field from the neighboring grains becomes smaller with a smaller grain size, β becomes smaller with a smaller grain size. Because of this low-temperature coefficient of coercivity, the eutectic diffusion-processed hot-deformed magnet shows a relatively high coercivity of 0.5 T even at 200 °C. For these applications, a room-temperature coercivity higher than 2.5 T is desired. Note that the platelet-like grains are still interconnected in the longitudinal direction, as shown in Figure 2(c). Thus, if we are able to decouple the exchange in the longitudinal direction, a coercivity of ∼2.5 T would be achievable.

A noteworthy property is the energy density, $(BH)_{max}$, of the diffusion-processed hot-deformed magnets at elevated temperature, as shown in Figure 4(b). Although the $(BH)_{max}$ of the original hot-deformed magnets shows large degradation compared to those of the Dy-containing sintered magnets, the hot-deformed magnet that was diffusion-processed with the expansion constraint shows relatively little temperature degradation compared to the original hot-deformed magnet. The temperature dependence is similar to those of the 4% Dy and 8% Dy sintered magnets, but its room-temperature $(BH)_{max}$ is larger than those of the Dy-containing sintered magnets. Thus, we can conclude that the $(BH)_{max}$ at 200 °C of the eutectic-diffusion-processed magnets with the expansion constraint is larger than those of the Dy-containing high-coercivity sintered magnets.

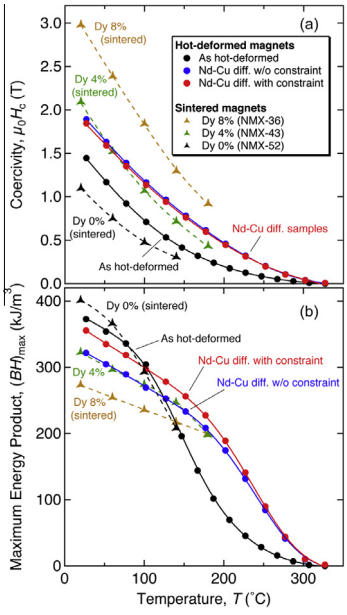

Figure 4. Temperature dependence of: (a) the coercivity and (b) the energy density of the hot-deformed magnet and the samples that were $Nd_{70}Cu_{30}$ diffusion-processed with and without an expansion constraint. For comparison, the energy densities of commercial 4% Dy and 8% Dy sintered magnets are also shown. The data for the commercial magnets were extracted from Ref. [18].

In summary, we have developed a low-temperature eutectic diffusion process with an expansion constraint as a method to achieve high-coercivity and high-energy-density Dy-free Nd–Fe–B magnets for high-temperature applications. The hot-deformed magnet that was treated with the low-temperature eutectic diffusion process under the constraint of expansion shows $\mu_0 H_c \sim 2$ T, $\mu_0 M_r = 1.36$ T and $(BH)_{max} = 358$ kJ m^{-3} at room temperature. Because of the low-temperature coefficient of coercivity for the ultrafine grain size, a $(BH)_{max}$ of 191 kJ m^{-3} was achieved at 200 °C. This Dy-free magnet outperforms the 4% Dy-containing (Nd,Dy)–Fe–B sintered magnet.

This work was supported by Japan Science and Technology Agency, CREST.

[1] R. Ramesh, G. Thomas, B.M. Ma, J. Appl. Phys. 64 (1988) 6416.
[2] P. Nothnagel, K.H. Müller, D. Eckert, A. Handstein, J. Magn. Magn. Mater. 101 (1991) 379.
[3] K. Uestuener, M. Katter, W. Rodewald, IEEE Trans. Magn. 42 (2006) 2897.
[4] K. Hono, H. Sepehri-Amin, Scripta Mater. 67 (2012) 530.
[5] M. Sagawa, Proceedings of the 21st Workshop on Rare-Earth Permanent Magnets and their Applications, Bled, 29 August 2010, pp. 183–186.
[6] R.W. Lee, E.G. Brewer, N.A. Schaffel, IEEE Trans. Magn. MAG-21 (1985) 1958.
[7] W.F. Li, T. Ohkubo, K. Hono, Acta Mater. 57 (2009) 1337.
[8] J. Liu, H. Sepehri-Amin, T. Ohkubo, K. Hioki, A. Hattori, T. Schrefl, K. Hono, Acta Mater. 61 (2013) 5387.
[9] C.D. Fuerst, E.G. Brewer, Appl. Phys. Lett. 56 (1990) 2252.
[10] C.D. Fuerst, E.G. Brewer, J. Appl. Phys. 69 (1991) 5826.
[11] F.E. Pinkerton, C.D. Fuerst, J. Magn. Magn. Mater. 89 (1990) 139.
[12] H. Sepehri-Amin, T. Ohkubo, T. Nishiuchi, S. Hirosawa, K. Hono, Scripta Mater. 63 (2010) 1124.
[13] C. Mishima, K. Noguchi, M. Yamazaki, H. Mitrai, Y. Honkuta. Proceedings of the 21st Workshop on Rare-Earth Permanent Magnets and their Applications, Bled, 29 August 2010, p. 253.
[14] H. Sepehri-Amin, T. Ohkubo, S. Nagashima, M. Yano, T. Shoji, A. Kato, T. Schrefl, K. Hono, Acta Mater. 61 (2013) 6622.
[15] H. Sepehri-Amin, J. Liu, T. Ohkubo, K. Hioki, A. Hattori, K. Hono, Scripta Mater. 69 (2013) 647.
[16] T. Akiya, J. Liu, H. Sepehri-Amin, T. Ohkubo, K. Hioki, A. Hattori, K. Hono, J. Appl. Phys. (2014), http://dx.doi.org/10.1063/1.4869062.
[17] S. Hirosawa, A. Hanaki, H. Tomizawa, A. Hamamura, Phys. B 164 (1990) 117.
[18] <http://www.hitachi-metals.co.jp/products/auto/el/pdf/nmx.pdf>.